Acoustic pulse propagation above grassland and snow: Comparison of theoretical and experimental waveforms

Donald G. Albert
U.S. Army Cold Regions Research and Engineering Laboratory, 72 Lyme Road, Hanover, New Hampshire 03755-1290

John A. Orcutt
Institute of Geophysics and Planetary Physics (A-025), Scripps Institute of Oceanography, La Jolla, California 92093

(Received 12 January 1989; accepted for publication 1 September 1989)

Theoretical predictions are made of the effect of an absorbing ground surface on acoustic impulsive waveforms propagating in a homogeneous atmosphere for frequencies below 500 Hz. The lower frequencies of the pulse are enhanced as the effective flow resistivity of the ground surface decreases and as the propagation distance increases. The pulse waveforms and peak amplitude decay observed for propagation distances of 40 to 274 m over grassland were satisfactorily matched by calculations using an assumed effective flow resistivity of 200 kN s m^{-4}. Measurements over snow gave much greater amplitude decay rates, and the waveforms were radically changed in appearance, being dominated by the lower frequencies. These waveforms were satisfactorily matched only when a layered ground was incorporated into the calculations; then, an assumed surface effective flow resistivity of 20 kN s m^{-4} gave good agreement with the observed waveforms and peak amplitude decay.

PACS numbers: 43.28.Fp, 43.40.Ph

INTRODUCTION

The absorption of sound energy by the ground has been studied extensively[1-5] because of its importance in understanding noise propagation through the atmosphere. Predictions of outdoor sound levels produced by various sources can be usefully applied to practical problems such as the reduction of traffic or industrial noise, and the estimation of community nuisance or damage levels from artillery firing ranges, construction blasting, and other explosions. These predictions are also of interest in estimating acoustic-to-seismic coupling phenomena, which was our main reason for undertaking this study. In all of these applications, ground absorption is a major factor determining the overall sound level. Most studies have reported ground absorption effects as a function of frequency in terms of excess attenuation, the ratio of the sound level with the ground present to the sound level in free space at the same propagation range, expressed in decibels. Only a few studies[6-8] have dealt with the effect of the ground on acoustic pulse propagation, which requires integration over the frequency bandwidth of interest.

In this article, we report on calculations and measurements of the absorption effects of snow-covered ground on acoustic pulse propagation. Acoustic propagation above snow has been studied in the past, although infrequently[4,9] (and additional references in Ref. 9), and primarily using continuous rather than impulsive sources. Gubler[10] did make some impulse measurements over snow, but reported only the amplitude decay rates observed and did not make waveform comparisons. Our study differs from previous studies of pulse propagation in two ways: First, we calculate absorption effects using a physically based theoretical model of finite ground impedance, the four-parameter model of Attenborough,[1] and compare these calculations to those using the semiempirical, single-parameter model of Delaney and Bazley[11] that has been used in past work; and second, we compare the model predictions with measurements over snow-covered ground. Apparently, this is the first report of extensive impulse measurements over such a highly absorptive geological boundary.

In Sec. I, we outline the theory used to describe the effect of an absorbent boundary on acoustic waves and models that are used to estimate the absorbing characteristics of the ground. Section II discusses the method used to predict the pulse waveforms expected after propagation along an absorbing boundary. In Sec. III, we present some examples of calculated waveforms and make comparisons with data obtained for propagation over grassland and over snow. We also compare the predicted and observed amplitude decay as a function of range for these two ground surfaces. Section IV summarizes our results.

I. THEORY

A. Effect of an absorbing boundary

The well-known expression (e.g., Refs. 2, 4, 6, and 12) for the pressure P received at a height h_r above an impedance boundary from a continuously emitting point source at a height h_s and a distance r_1 away (Fig. 1) is given by

$$\frac{P}{P_0} = \frac{1}{k_1 r_1} e^{ik_1 r_1} + \frac{1}{k_1 r_2} Q e^{ik_1 r_2}, \tag{1}$$

where P_0 is a reference pressure level near the source, k_1 is the wavenumber in the air, and r_1 and r_2 are the direct and reflected waves' pathlengths. The first term in Eq. (1) gives the pressure from the direct wave; the second gives the contribution from the boundary. The dimensionless image

 0001-4966/90/010093-08$00.80

source strength Q is defined to include the reflection from the boundary and the ground-wave term:

$$Q = R_p + (1 - R_p)F(w), \tag{2}$$

where the plane-wave reflection coefficient R_p is

$$R_p = (Z_2 \sin\phi - Z_1 s^{1/2})/(Z_2 \sin\phi + Z_1 s^{1/2}), \tag{3}$$

with Z_1 and Z_2 representing the specific acoustic impedances of the two media, ϕ the angle of incidence defined in Fig. 1, and

$$s = 1 - (k_1/k_2)^2 \cos^2\phi. \tag{4}$$

A steepest-descent approach[12] can be used to evaluate F and gives

$$F(w) = 1 + i(\pi)^{1/2} w e^{-w^2} \operatorname{erfc}(-iw), \tag{5}$$

where the dimensionless numerical distance w is defined by

$$w^2 = 2ik_1 r_2 (1 - R_p)^{-2} (Z_1/Z_2)^2. \tag{6}$$

The steepest-descent derivation involves a high-frequency approximation, which requires that

$$kr \gg 1, \tag{7}$$

or, equivalently,

$$f \gg c/(2\pi r), \tag{8}$$

where f is the frequency in Hz and c the acoustic wave speed. This limiting frequency value is 5 Hz for a 10-m propagation range in air, and 1 Hz for 40 m, the shortest propagation range for the measurements reported on here.

The equations were derived using a local reaction condition, which assumes that the surface acoustic impedance of the boundary is independent of the incident angle (or, equivalently, that the transmitted waves are refracted vertically into the lower medium). The assumptions that the waves arrive at grazing incidence and that $|Z_2| > |Z_1|$ were also used in the derivation.

In all of our calculations, we have assumed a homogeneous atmosphere (i.e., no refraction of acoustic rays) without turbulence. We have omitted atmospheric absorption from the calculations, since Don and Cramond's[6] and our own calculations have shown that it is negligible at these ranges (<300 m) and frequencies (<500 Hz). The next section discusses the models that we used to determine the ground impedance Z_2 needed for the calculation of pulse waveforms via Eqs. (3) and (6).

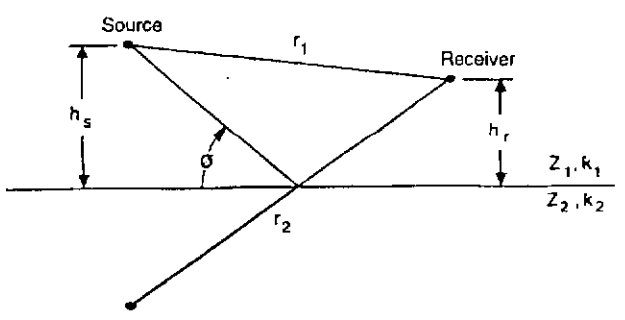

FIG. 1. Geometry of the calculations and observations. The two acoustic media have impedances and propagation consants of Z_1, k_1 and Z_2, k_2, respectively. The source and receiver are both in medium 1, at heights of h_s and h_r, and the direct and reflected wave pathlengths are r_1 and r_2. The angle of incidence is ϕ.

B. Models of ground impedance

Past predictions of acoustic pulse waveforms[6-8] have exclusively employed Delaney and Bazley's single-parameter model[11] of ground impedance. This model consists of the empirically determined relationships

$$R/\rho c = 1 + 0.05(f/\sigma)^{0.75}, \tag{9}$$

$$X/\rho c = 0.77(f/\sigma)^{-0.73}, \tag{10}$$

where R and X are the real and imaginary parts of the ground impedance Z_2, ρ is the density of the air, and σ is the flow resistivity of the porous ground. [The numerical constants in Eqs. (9) and (10), and in Eqs. (12) and (13) below, actually have units that cancel those of the (f/σ) terms, making the equations dimensionless.] Attenborough[13] pointed out that Delaney and Bazley[11] derived their model using materials for which the porosity was nearly 1 and gave a theoretical argument showing that the measured flow resistivity should be multiplied by the porosity before substitution into Eqs. (9) and (10). It is this value, termed the *effective* flow resistivity, that we denote by the symbol σ in this paper. Here, σ has units of N s m^{-4} or mks rayls m^{-1}. In this paper, we give numerical values in kN s m^{-4} ($= 10^3$ N s m^{-4}), which makes the values the same as those expressed in cgs units in some earlier papers.

The ground sometimes behaves like a layered porous medium, rather than the infinitely thick layer assumed in Eqs. (9) and (10). If we let d be the layer thickness and k_2 the wavenumber in the layer, then the resulting impedance of the medium is[14]

$$Z = Z_2(Z_3 - iZ_2 \tan k_2 d)/(Z_2 - iZ_3 \tan k_2 d), \tag{11}$$

where Z_2 and Z_3 are the impedances of the upper and lower materials, respectively, found using Eqs. (9) and (10). Delaney and Bazley[11] also determined formulas for the wavenumber $k_2 = \alpha + i\beta$ such that

$$\alpha/k_1 = 1 + 0.098(f/\sigma)^{-0.70}, \tag{12}$$

$$\beta/k_1 = 0.19(f/\sigma)^{-0.59}. \tag{13}$$

The second model of ground impedance that we use in our calculations was developed by Attenborough.[1] This model treats the porous medium as a rigid frame with randomly varying pore sizes. The model requires four parameters to describe the material: effective flow resistivity σ, porosity Ω, grain shape factor n', and pore shape factor ratio s_f. Propagation in the porous medium is then described by [Eqs. (8) and (9) in Ref. 1]

$$k_2^2 = q^2[1 - 2u^{-1}T(u)]^{-1} \times [1 + 2(\gamma - 1)v^{-1}T(v)](\omega/c)^2, \tag{14}$$

$$Z_c = q^2[1 - 2u^{-1}T(u)]^{-1}(1/k_2\Omega), \tag{15}$$

with the following definitions: q^2 = tortuosity $= \Omega^{-n'}$ (dimensionless), γ = ratio of specific heats, $\omega = 2\pi f$, $T(x) = J_1(x)/J_0(x)$ = ratio of cylindrical Bessel functions, $\lambda = (1/s_f)[8\rho q^2\omega/\Omega\sigma]^{1/2}$, $u = \lambda i^{1/2}$, $v = N_{Pr}^{1/2}u$, and N_{Pr} = Prandtl number. The impedance of a layered medium is determined by Eqs. (11), (14), and (15). In all of the computations, we have set $n' = 0.5$, and we have taken $N_{Pr} = 0.712$ and $\gamma = 1.4$ for air. Most of the other values were

taken from measurements reported by Attenborough for soils[1] and by Attenborough and Buser for snow.[15,16]

With the definition $\sigma_e = s_f^2\sigma/\Omega$, Attenborough[1] also obtained a low-frequency approximation of the four-parameter model that requires only two parameters:

$$Z_c = (4\pi\gamma\rho)^{-0.5}(\sigma_e/f)^{0.5}(1+i), \tag{16}$$

$$k_2 = Z_c\gamma\Omega. \tag{17}$$

II. CALCULATION OF PULSE WAVEFORMS

In the following equations, lower case letters denote sampled quantities in the time domain and upper case letters denote the corresponding frequency domain values. Here, m and n are used as subscripts for the particular index value in the time and frequency domain.

The sampled source pulse is given by the sequence $\{s_m\}$, $m = 0,1,...,N-1$, with an interval of Δt s between samples. The source pulse components in the frequency domain are found by taking the discrete Fourier transform

$$S_n = \sum_{m=0}^{N-1} s_m e^{i2\pi mn/N}, \quad n = 0,1,...,N-1. \tag{18}$$

The elements of the complex sequence $\{S_n\}$ occur at frequency values $f_n = n/(N\Delta t)$; i.e., the frequency spacing is $\Delta f = 1/(N\Delta t)$ and the highest is $f_N = 1/(2\Delta t)$. The image response Q_n is computed at all of the desired frequencies using either the single-parameter[11] model, the four-parameter[1] model, or its low-frequency approximation. The resultant X_n of the direct and reflected pulse is then

$$X_n = S_n[(4\pi r_1)^{-1}\exp(i2\pi f_n r_1/c) + (4\pi r_2)^{-1}\exp(i2\pi f_n r_2/c)Q_n]. \tag{19}$$

For a receiver at the surface, $r_2 = r_1$ $(= r)$, and so Eq. (19) becomes

$$X_n = (4\pi r)^{-1}S_n(1+Q_n)\exp(i2\pi f_n r/c). \tag{20}$$

In the above equation, the exponential term is merely a phase delay that determines the arrival time of the pulse. This term was replaced by $\exp(i2\pi f_n t_0)$ in the computations, where t_0 is a fixed time shift. This replacement is equivalent to the use of a reduction velocity to align the pulses for all ranges at the time t_0 and avoids the need to compute additional terms as the range increases.

Next, a window is applied to limit the calculations to the recording system's bandwidth of 500 Hz. The window coefficients we used reproduce the effect of the recording system's antialiasing filter and are given by

$$W_n = \sin^4[(n-1)\pi/N], \quad n = 0,1,...,N-1. \tag{21}$$

The resultant pulse in the frequency domain then becomes

$$X_n = (1/4\pi r)W_n S_n(1+Q_n)\exp(i2\pi f_n t_0). \tag{22}$$

The time domain pulse x_m was then computed from Eq. (22) using the inverse discrete Fourier transform:

$$x_m = \frac{1}{N}\sum_{n=0}^{N-1} X_n e^{-i2\pi mn/N}, \quad m = 0,1,...,N-1. \tag{23}$$

In all of the computations, the recording system's sampling interval of $\Delta t = 0.5$ ms was used. The fast Fourier transform (FFT) algorithm was used to compute Eqs. (18) and (23), with the number of points N set to 2048, and so $\Delta f = 0.997$ Hz and $f_N = 1$ kHz. Since Q_n turns out to vary smoothly, a wider frequency spacing could probably have been used, and direct integration without the use of the FFT algorithm may be more efficient. For all of the calculations, the source height was set to 1 m, and the receiver was on the surface.

III. RESULTS AND DISCUSSION

A. Theoretical examples

We first calculate two examples, chosen to illustrate the extremes in the importance of the ground impedance on propagating acoustic pulses. The first is presented in Figs. 2 and 3. The single-parameter impedance model[11] was used,

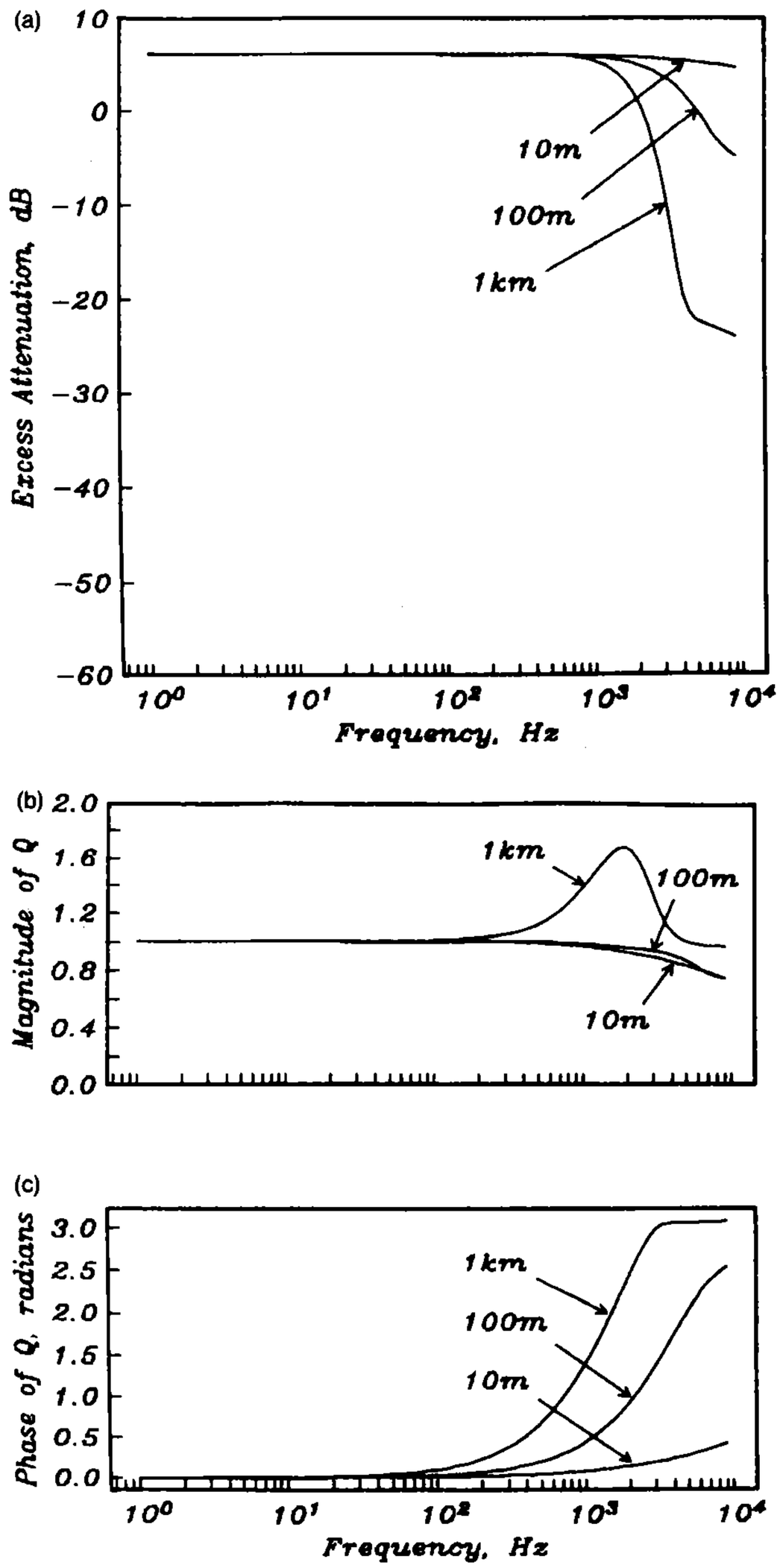

FIG. 2. (a) Excess attenuation, (b) image source magnitude, and (c) image source phase as a function of frequency calculated using the Delaney and Bazley model (Ref. 11) with $\sigma = 32\,000$ kN s m^{-4}. Propagation distances are 10, 100, and 1000 m, source height 1 m, and receiver at the surface.

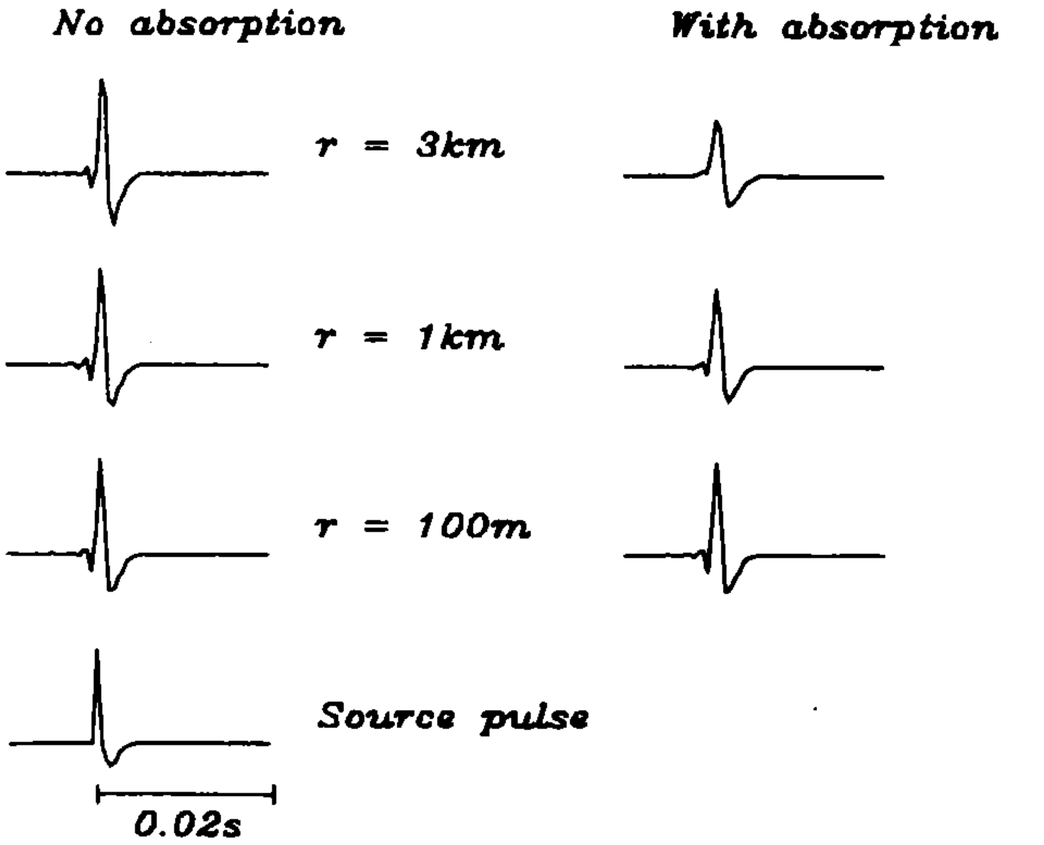

FIG. 3. Waveforms calculated using the Delaney and Bazley model (Ref. 11) with $\sigma = 32\,000$ kN s m^{-4} for ranges of 0.1, 1, and 3 km. Source height 1 m, receiver at the surface. The source pulse used is shown at the bottom of the figure, and the spectrum is bandlimited to 500 Hz. The waveforms on the left were calculated ignoring the effects of atmospheric absorption; those on the right include absorption. The waveforms on the left are normalized; the peak amplitudes are 2000, 33, 3, and 1 Pa, respectively, from bottom to top. The waveforms on the right are plotted at the same scale as those on the left, and they have peak amplitudes of 32, 2.5, and 0.6 Pa.

with σ set to 32 000 kN s m^{-4}, a value representative of an old asphalt surface[4] and of the highest value the effective flow resistivity could be expected to reach for outdoor propagation. Figure 2 shows the excess attenuation and the magnitude and phase of the image source [Q in Eq. (2)], calculated at propagation distances of 10, 100, and 1000 m. The high effective flow resistivity value used specifies an acoustically hard surface, and the response is generally flat up to 1 kHz, implying that very little waveform change will occur. Figure 3 shows the calculated waveforms, using the source waveform shown, for ranges up to 3 km. The source waveform used in this and in all of the following calculations is an estimated one, because our measurements from microphones close to the source were clipped. We estimated the peak amplitude of the experimental pulse as 2 kPa at 1 m.

Two sets of waveforms are shown in Fig. 3, one set with and one set without air absorption.[17] The pulse waveforms are virtually identical at all propagation distances when air absorption is ignored. When absorption is included, the peak amplitudes are lower and the waveforms are slightly broader. The amplitude reduction is only a few percent at 100 m and about 20% at 1 km.

The next calculation used $\sigma = 10$ kN s m^{-4}, a value representing a very absorptive surface like snow,[9] near the lower bound of effective flow resistivity. The excess attenuation and image source curves shown in Fig. 4 now exhibit a more complicated structure in the frequency band of interest. At low frequencies, the boundary is fully reflecting, and the sound level is double that of the free-space value, with a corresponding excess attenuation value of $+6$ dB. The attenuation begins to increase at higher frequencies, reaching 0 dB at 100, 45, and 20 Hz for propagation distances of 10, 100, and 1000 m. This decay arises from the phase change that occurs on reflection from the boundary.

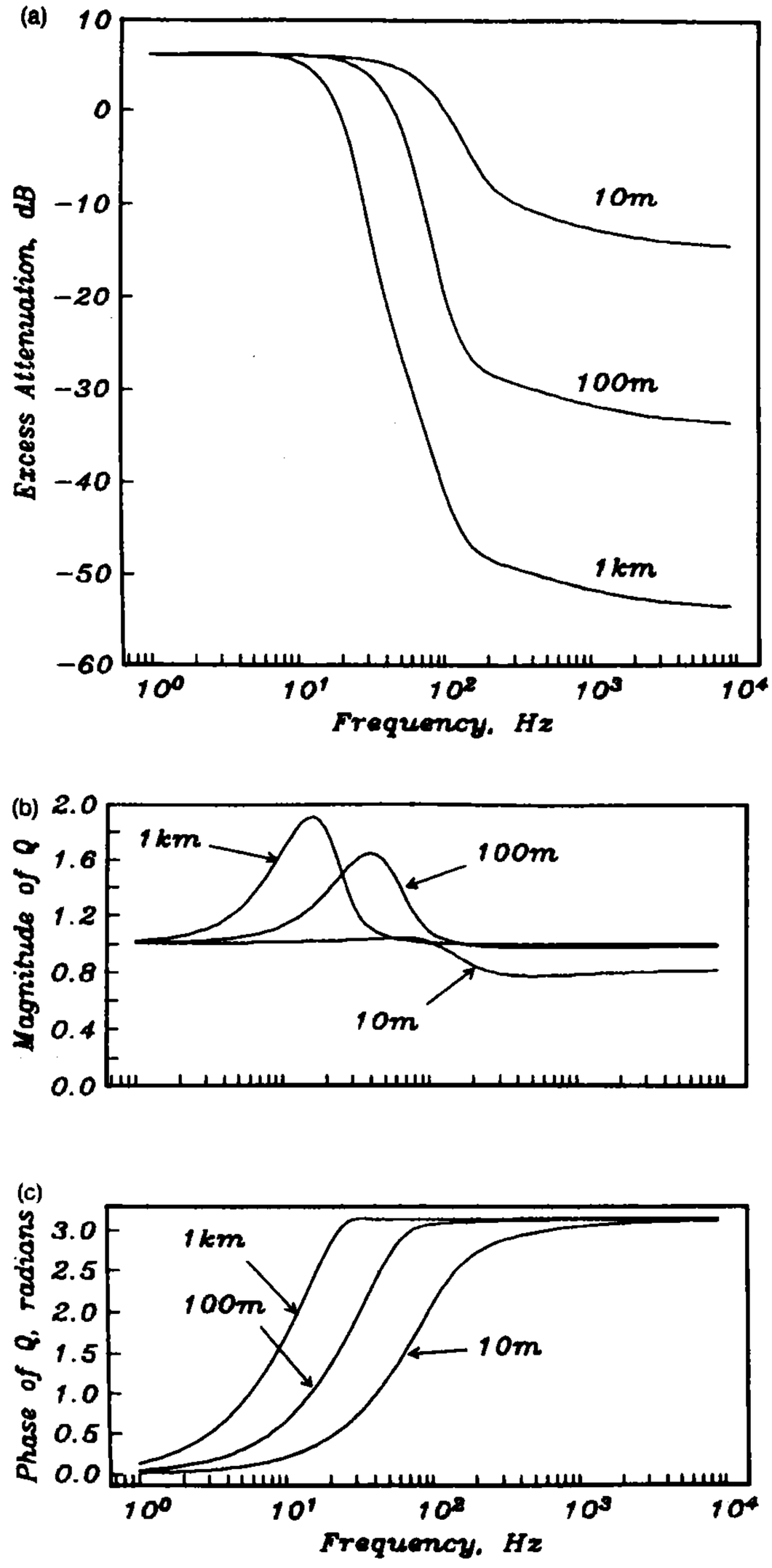

FIG. 4. (a) Excess attenuation, (b) image source magnitude, and (c) image source phase as a function of frequency calculated using the Delaney and Bazley model (Ref. 11) with $\sigma = 10$ kN s m^{-4}. Same source and receiver geometry as in Fig. 3.

The effects of the low effective flow resistivity surface on propagating acoustic pulse shapes are shown in Fig. 5. The pulse amplitudes are much lower than in the previous example, and low frequencies dominate and elongate the waveform for ranges beyond a few tens of meters. This enhancement of the lower frequencies is the result of integrating over the image source magnitude shown in Fig. 4(b), with the dominant frequencies of the waveforms at 100 and 1000 m, corresponding to the peak image source magnitudes at 40 and 15 Hz. Figure 5 also displays two sets of waveforms, calculated with and without air absorption. In this case, the waveforms are nearly identical, even at a range of 3 km,

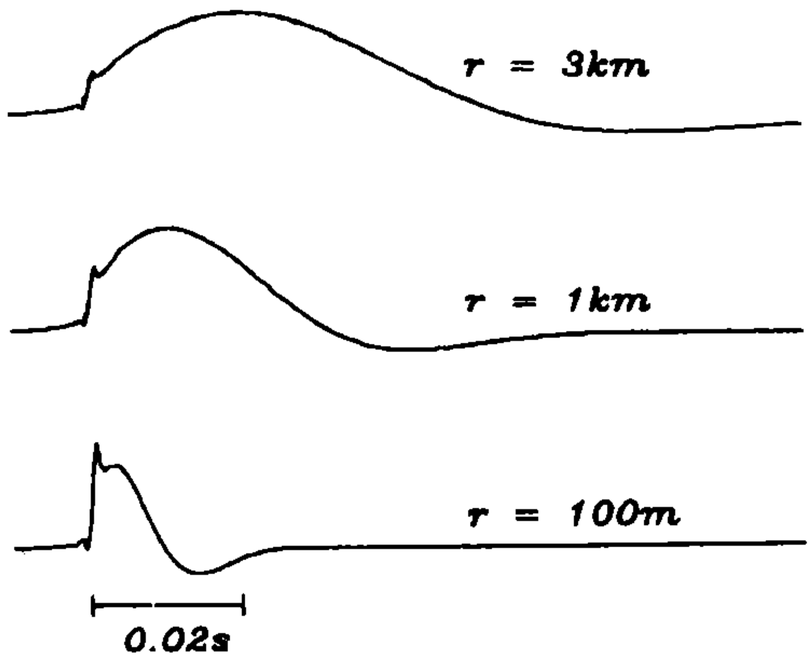

FIG. 5. Waveforms calculated using the Delaney and Bazley model (Ref. 11) with $\sigma = 10$ kN s m^{-4} for ranges of 0.1, 1, and 3 km. The source pulse used is shown in Fig. 3. The waveforms shown as solid lines ignore the effect of atmospheric absorption. Waveforms that were calculated including the absorption effects were identical to those calculated in the absence of air absorption at this scale. The peak amplitudes are 1.5 Pa at 100 m, 0.03 Pa at 1 km, and 0.005 Pa at 3 km.

because the low frequencies that dominate these pulses are not greatly affected by air absorption.

These examples show that hard boundaries, i.e., those with a high effective flow resistivity, act as good reflectors and have little effect on pulse waveforms, while soft, absorbent boundaries with low effective flow resistivities can produce radically different waveforms by absorbing the higher frequencies. Additional calculations (omitted here) revealed that the three other parameters involved in Attenborough's model have an influence on the waveforms smaller than that of the effective flow resistivity. This explains the success of the Delaney and Bazley model in past work; it concentrates on the most important parameter, the effective flow resistivity. In the next section, we show that calculated waveforms using either of the models can successfully match the waveforms observed in outdoor sound propagation experiments.

B. Observations and waveform comparisons

Recordings of acoustic pulses propagating distances up to 274 m under summer and winter conditions were obtained at a firing range in northern Vermont. The site was relatively flat, sloping generally upward from west to east. The subsurface consisted of a 15- to 25-m-thick layer of unconsolidated soil, mostly silty sands with some gravel, which became saturated at a depth of 0.4 m. In the summer, the ground was covered with 0.2-m-tall grass; a snow cover varying between 0.15 and 0.32 m in depth above a 0.03-m-thick frozen soil layer was present in the winter. Geophones and microphones were placed 3 m apart along the ground surface, and 0.45 caliber blank pistol shots were fired toward the sensors from a height of 1 m. The 24 signal channels were sampled at a rate of 2 kHz by a digital recording system with a frequency bandwidth of 500 Hz. Additional details are given in Ref. 18.

The summer recordings occurred under homogeneous atmospheric conditions with a slight breeze blowing perpendicular to the propagation path. A strong inversion was present during the winter experiments ($dT/dz = +4$ to $+1$ K m^{-1}), but the expected amplitude enhancement from refraction was overwhelmed by the strong absorption of acoustic energy by the snow cover as the data below will show. The snowpack consisted of five distinct layers, with measured densities from 190 to 290 kg m^{-3}, and crystal sizes ranging from 0.1–2 mm. The most recent snowfall of about 0.04 m had occurred 3 days before the experiments.

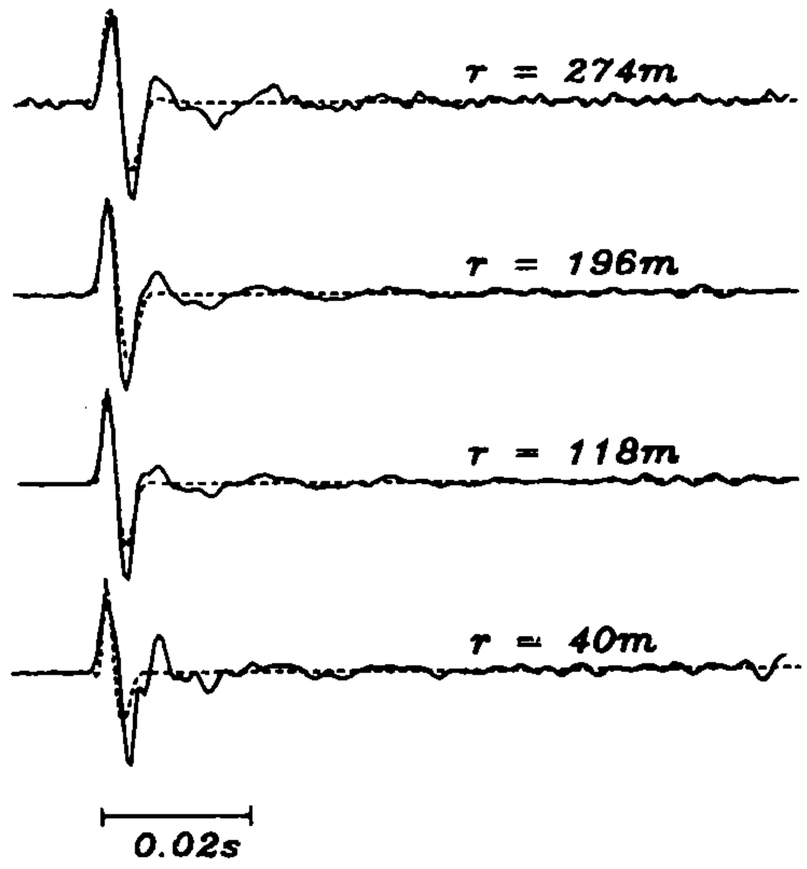

FIG. 6. Comparison of normalized waveforms for pulse propagation over grassland for ranges from 40–274 m. The solid lines are the waveforms recorded by surface microphones, and the observed peak amplitudes were 12, 9.1, 4.6, and 2.0 Pa, respectively, from bottom to top. The dashed lines are waveforms calculated using the Delaney and Bazley model (Ref. 11) with $\sigma = 200$ kN s m^{-4}. For the calculated waveforms, the source pulse shown in Fig. 3 was used, and the spectrum is limited to 500 Hz.

Figure 6 shows typical summer surface microphone recordings (solid line) for a series of pistol shots at ranges from 40–274 m. These shots were recorded during a 75-min period by moving the source farther away from the receivers in an eastward direction. We ran a number of sample calculations using the single-parameter model in a trial-and-error forward modeling process and found that a value of $\sigma = 200 \pm 50$ kN s m^{-4} gave good agreement with the observed pulse waveforms. The calculated waveforms are shown as dashed lines in Fig. 6.

Typical waveforms observed in the winter by microphones at the snow surface are shown as solid lines in Fig. 7. These recordings were made at the same locations as the summer measurements and were obtained over a 130-min period. The waveforms are markedly different from those observed in the summer, but show some of the same properties of the waveforms calculated with $\sigma = 10$ kN s m^{-4} that were displayed in Fig. 5: The high-frequency portion of the pulse is severely attenuated, and the lower frequencies become increasingly dominant as the propagation range increases. The complicated high-frequency pulse shapes near the beginning of the waveforms in Fig. 7 are due to reflections from within the snowpack.

Modeling of these waveforms was unsuccessful without the addition of a hard layer beneath the snow. In fact, the best match with an unlayered ground was achieved by the waveforms shown in Fig. 5. Nicolas *et al.*[9] found that they required a layered ground to fit their measurements of excess attenuation over snow at much shorter ranges and at higher

frequencies. We also achieved much better results when the ground was modeled as a layer over a half-space.

The short dashed line in Fig. 7 shows the best waveform match achieved using the single-parameter model with a hard subsurface layer. The upper and lower effective flow resistivities were 20 and 366 kN s m^{-4}, respectively, and the layer thickness was 0.15 m. The surface effective flow resistivity was determined by matching the decay of the high-frequency pulses and the layer thickness by matching the elongation of the waveform. Estimated errors are 10 kN s m^{-4} for the effective flow resistivity and 0.05 m for the layer thickness. Slightly better results were achieved using the four-parameter model with the same effective flow resistivities (the long dashed lines in Fig. 7). The assumed porosities and pore shape factor ratios were $\Omega = 0.7$ and $s_f = 0.8$ for the snow, and $\Omega = 0.269$ and $s_f = 0.725$ for the hard underlying soil.[19] The overall elongated shape of the waveform and its relative amplitude in comparison to the higher frequency pulses match the observed data slightly better than the results using the single-parameter model. For both models, the snow layer thickness of 0.15 m was less than the thickness of 0.25 m directly beneath the microphone, but close to the average thickness of 0.19 m along the propagation path. Calculated waveforms using the low-frequency approximation [Eqs. (16) and (17)] were identical to the waveforms for the four-parameter model and have been omitted from the plot.

The data presented here have shown that propagation over an absorptive ground like snow can greatly modify pulse waveforms by attenuating the higher frequencies. Our calculations show that any of the three models can be used to calculate waveforms that agree satisfactorily with the observed changes.

C. Amplitude decay rate comparisons

Along with waveform comparisons, the observed pulse amplitude decay as a function of propagation distance can also be compared with the calculated values. The most direct way of comparing the decay rates is to use the microphone observations; however, many of the amplitudes on our microphone recordings, especially at the shorter propagation ranges and in the summer, exceeded the dynamic range of the microphones and were thus unreliable. We also used geophones in our experiments, and data from these sensors do not exhibit the clipping problems that the microphones do. In addition, many more geophones were available to us (since they are one-tenth the cost of the microphones), and the larger number used provides a better estimate of the amplitude decay. The geophones respond to the direct air pulse that propagates in the atmosphere and is locally coupled into the ground. We used our estimated source amplitude of 2 kPa at 1 m and the measured[18] acoustic-to-seismic coupling ratio of 6×10^{-6} m s^{-1} Pa^{-1} (the ratios were nearly the same for grassland and snow) to convert the calculated pressure amplitudes to particle velocity for comparison with the geophone measurements.

Figure 8 shows that the frequency response curves for a microphone and a geophone at the ground surface are very similar. These curves were obtained using a pistol shot 196 m away where the microphone responds without clipping; the recording was made in the summer. The microphone and geophone curves have about the same bandwidth. The dip caused by a 60-Hz notch filter used during the recording is visible in the microphone curve, as well as two noise peaks at about 420 and 540 Hz. The notch filter dip is also visible in

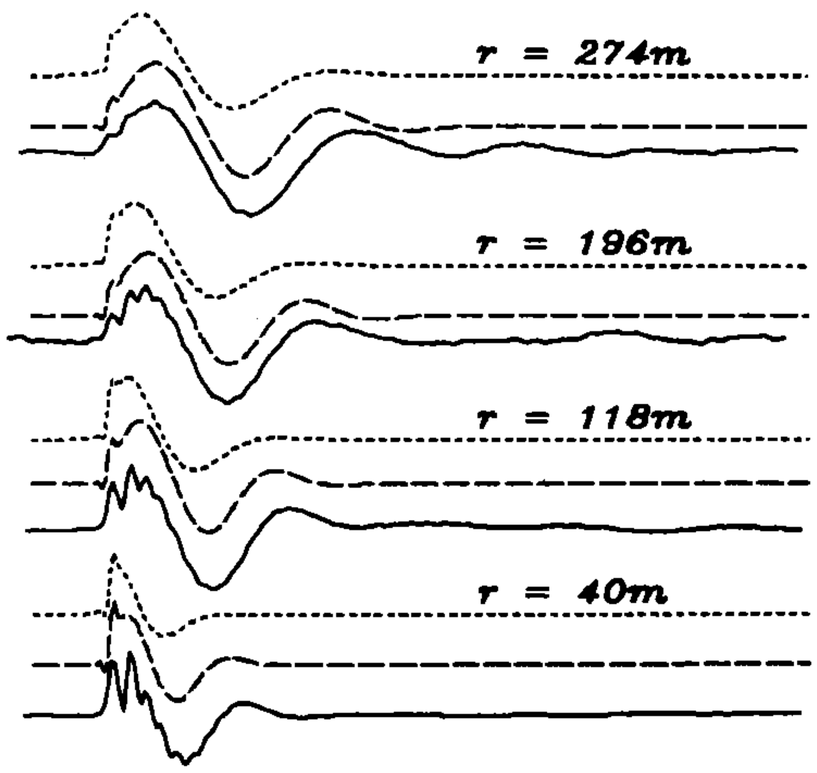

FIG. 7. Comparison of normalized waveforms for pulse propagation over snow for ranges from 40–274 m. The solid lines are the waveforms recorded by surface microphones, and the observed peak amplitudes were 5.1, 0.91, 0.60, and 0.17 Pa, respectively, from bottom to top. The long dashed lines above the solid lines are waveforms calculated using Attenborough's model (Ref. 1) for a layered ground. The first layer was 0.15 m thick and had parameter values of $\sigma = 20$ kN s m^{-4}, $\Omega = 0.7$, $s_f = 0.8$, and $n' = 0.5$. The underlying material had values of $\sigma = 366$ kN s m^{-4}, $\Omega = 0.269$, $s_f = 0.725$, and $n' = 0.5$. The short dashed lines are waveforms calculated using the Delaney and Bazley model (Ref. 11) for two layers with $\sigma = 20$ and 366 kN s m^{-4} and a layer thickness of 0.15 m. For the calculated waveforms, the source pulse shown in Fig. 3 was used, and the spectrum is limited to 500 Hz.

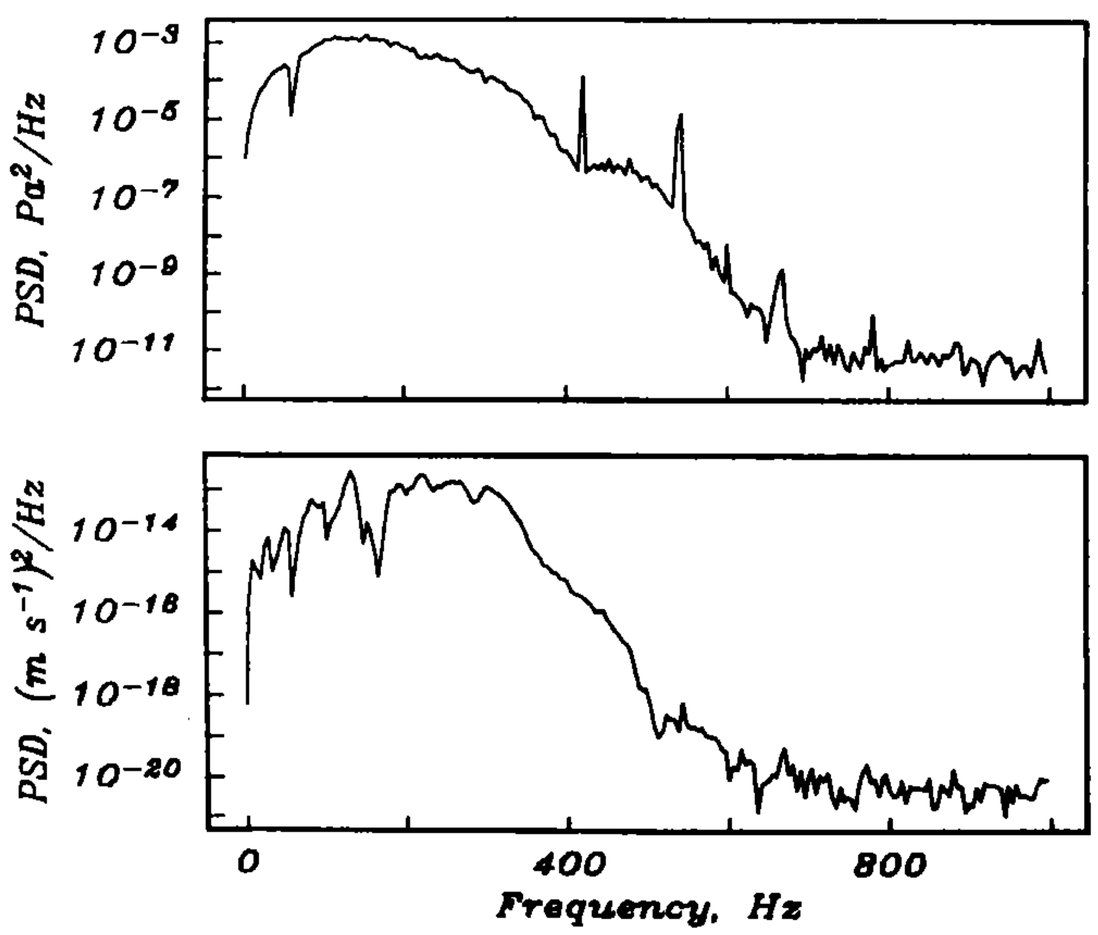

FIG. 8. Power spectral density (PSD) as a function of frequency for a surface microphone (top) and a surface vertical component geophone (bottom) in the summer. The source was a blank pistol shot 1 m above the ground and 196 m away from the sensors.

the geophone response curve, and the low-frequency portion of the curve (below 200 Hz) is much less smooth than for the microphone. Some of the roughness in the geophone spectrum is probably caused by the subsurface layering.[20] The pulse amplitudes are controlled by the integral over these response curves and will not be greatly affected by these differences.

Comparisons of observed and calculated pulse amplitudes as a function of propagation distance are presented in Figs. 9 and 10. In both figures, the symbols are observed measurements and the lines are calculated decay rates. The

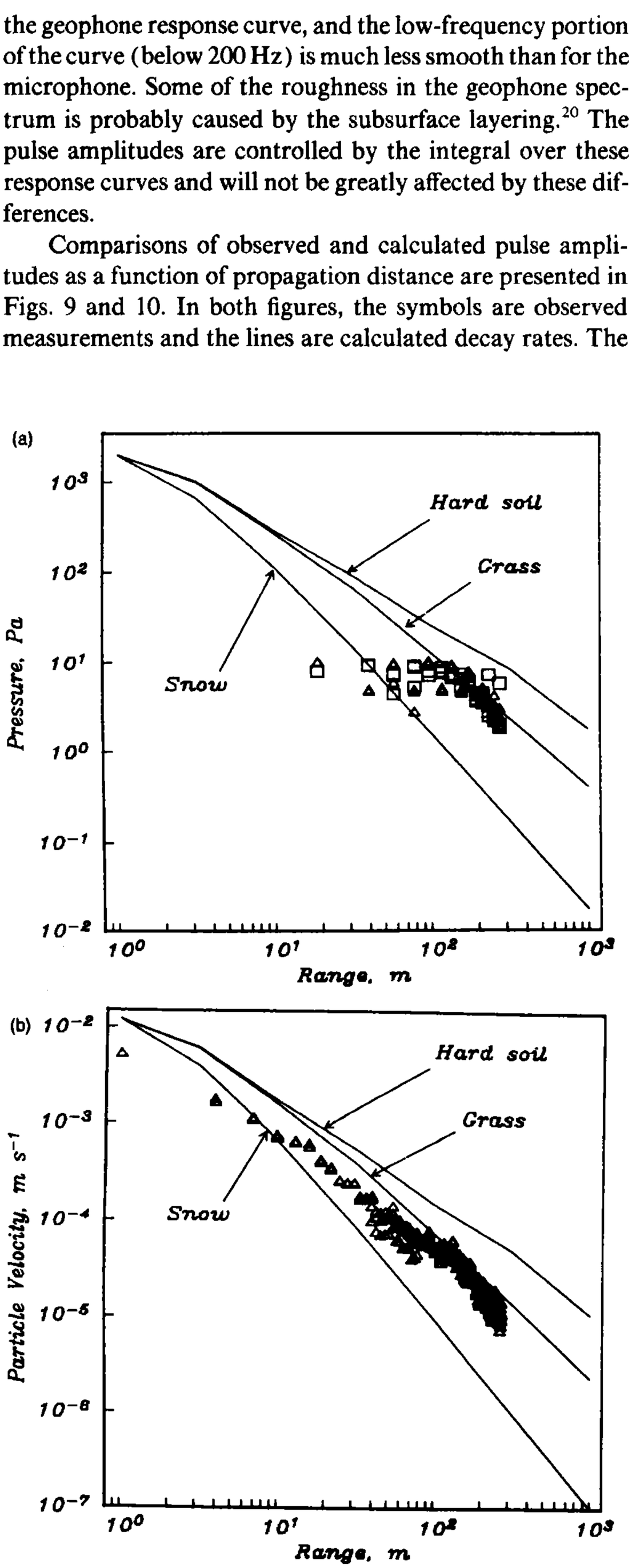

FIG. 9. Plot of first arrival amplitude versus distance from the source for pulse propagation over grassland. (a) Peak amplitudes from microphones; (b) peak amplitudes from vertical component geophones. Triangles denote amplitudes measured using receivers on the surface; squares are amplitudes measured using microphones 0.5 m high. The lines are amplitudes calculated using the Delaney and Bazley model (Ref. 11) with effective flow resistivities of 1820 (hard soil) and 200 kN s m^{-4} (grass). The line for snow was calculated using Attenborough's model (Ref. 1) with a surface effective flow resistivity of 20 kN s m^{-4} and the parameters listed in the caption for Fig. 7. The flat trend in the microphone amplitudes at the shorter ranges are the result of exceeding the dynamic range of the microphones (see text).

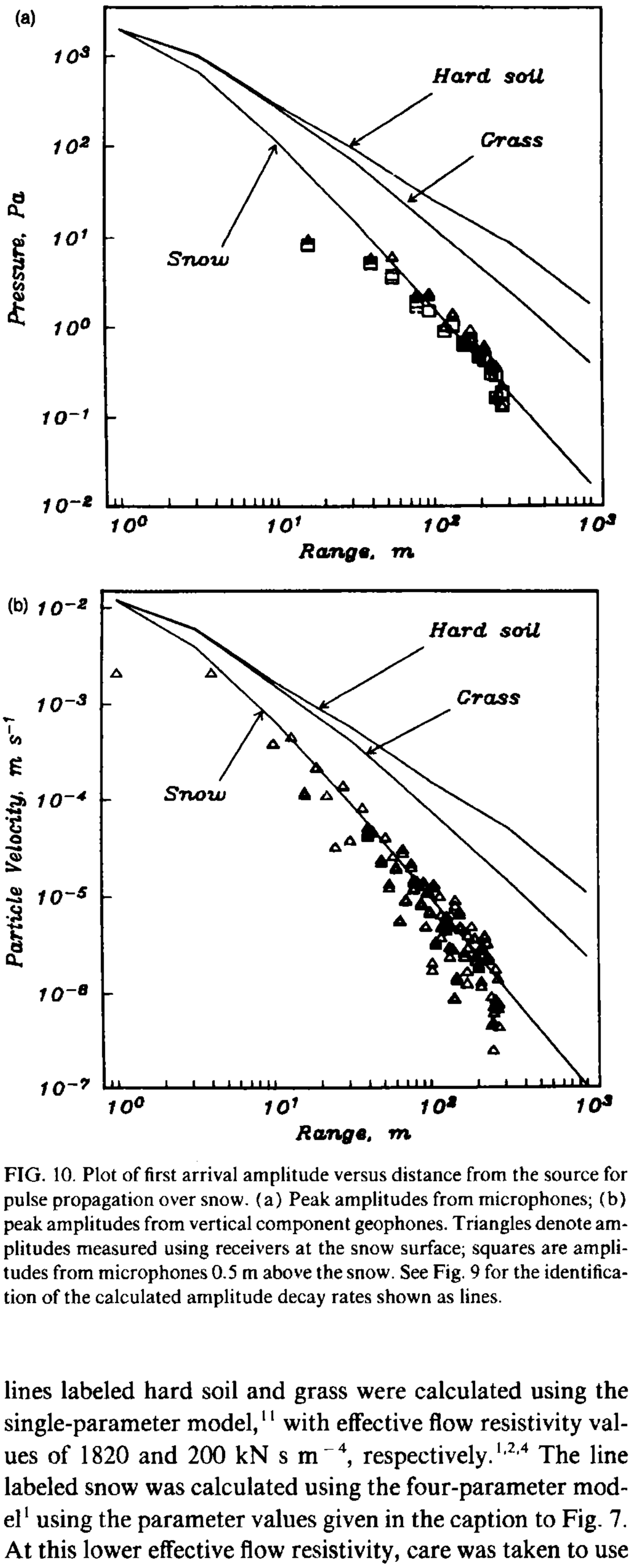

FIG. 10. Plot of first arrival amplitude versus distance from the source for pulse propagation over snow. (a) Peak amplitudes from microphones; (b) peak amplitudes from vertical component geophones. Triangles denote amplitudes measured using receivers at the snow surface; squares are amplitudes from microphones 0.5 m above the snow. See Fig. 9 for the identification of the calculated amplitude decay rates shown as lines.

lines labeled hard soil and grass were calculated using the single-parameter model,[11] with effective flow resistivity values of 1820 and 200 kN s m^{-4}, respectively.[1,2,4] The line labeled snow was calculated using the four-parameter model[1] using the parameter values given in the caption to Fig. 7. At this lower effective flow resistivity, care was taken to use the amplitude of the high-frequency pulse, not the low-frequency portion of the waveforms, as this is how the observed data are plotted.

Figure 9 shows the observed amplitudes in the summer. Ninety-two measurements were made with microphones, 320 with vertical component geophones. The plot shows that the microphone data are clipped until the propagation range exceeds 100 m; then, the amplitudes match those calculated for grass quite well. The geophone observations are slightly

lower than those calculated for grass, but decay at about the same rate. Considering all of the assumptions used to make these comparisons, the agreement is acceptable.

Figure 10 compares the observed amplitudes in the winter with the calculated amplitudes. Only a few of the 56 microphone amplitudes, those for ranges less than 40 m, may be clipped. The observations agree with the absolute amplitudes and with the decay rate calculated for snow. For the geophones, the agreement between the 126 observations and the calculated values is also very good.

IV. CONCLUDING REMARKS

Calculations have been used to investigate the effects of ground absorption on waveforms and amplitude decay for acoustic pulses. Hard grounds with high effective flow resistivities ($\sim 32\,000$ kN s m^{-4}) are good reflectors and absorb very little energy; consequently, in the absence of air absorption there is little change in the predicted waveforms for ranges up to 3 km. As the effective flow resistivity decreases (~ 200 kN s m^{-4}), absorption by the ground increases, and the pulse amplitudes decay faster as a function of range. At still lower effective flow resistivities (10–20 kN s m^{-4}), increased absorption and a change in the image source magnitude cause marked changes in waveforms, with the low frequencies dominating. A layered ground must then be used to correctly model the waveforms. Satisfactory agreement can be obtained between observed and calculated acoustic pulse waveforms and peak amplitude decay rates for two quite different ground surfaces, grassland and snow. The Delaney and Bazley model,[11] Attenborough's model,[1] and its low-frequency approximation all give good agreement with observations.

Our measurements, along with the calculated waveforms and amplitude decay rates, illustrate the silencing effect that a strongly absorbing snow layer has. The sound of the pistol shots was noticeably muffled to our ears during the winter experiments, and such quieting of sound levels is commonly observed when a snow layer is present. Since we have confirmed that both models can correctly account for these effects, they can be used with confidence in predicting acoustic pulse propagation over different ground conditions.

Future work will include both theoretical and experimental investigation of the effect of various snow cover properties and thicknesses on acoustic pulse propagation, and incorporation of temperature gradient and wind effects into the calculations. Another promising area worthy of further study is to relate stereologically measured parameters of snow[21] to the parameters needed for acoustic predictions, especially the pore shape factor ratio s_f and the grain shape factor n'.

ACKNOWLEDGMENTS

Keith Attenborough, Henry Bass, and James Sabatier supplied subroutines to calculate ground attenuation, and Keith Attenborough provided a manuscript copy of Ref. 15 in advance of publication. Valuable assistance with the field measurements was provided by Frank Perron and especially by Steve Decato. Steve Arcone and Ken Jezek provided useful comments or reviews. We also thank two anonymous reviewers and Louis Sutherland for many suggested improvements. This work is supported by the Directorate of Research and Development, U.S. Army Corps of Engineers, Projects 4A762730AT42 and AT24.

[1] K. Attenborough, "Acoustical impedance models for outdoor ground surfaces," J. Sound Vib. **99**, 521–544 (1985).
[2] C. I. Chessell, "Propagation of noise along a finite impedance boundary," J. Acoust. Soc. Am. **62**, 825–834 (1977).
[3] T. F. W. Embleton, J. E. Piercy, and N. Olson, "Outdoor sound propagation over ground of finite impedance," J. Acoust. Soc. Am. **59**, 267–277 (1976).
[4] T. F. W. Embleton, J. E. Piercy, and G. A. Daigle, "Effective flow resistivity of ground surfaces determined by acoustical measurements," J. Acoust. Soc. Am. **74**, 1239–1244 (1983).
[5] T. F. W. Embleton and G. A. Daigle, "Near-ground sound fields and surfaces of finite impedance," J. Acoust. Soc. Am. Suppl. 1 **82**, S76 (1987).
[6] C. G. Don, and A. J. Cramond, "Impulse propagation in a neutral atmosphere," J. Acoust. Soc. Am. **81**, 1341–1349 (1987).
[7] R. Raspet, H. E. Bass, and J. Ezell, "Effect of finite ground impedance on the propagation of acoustic pulses," J. Acoust. Soc. Am. **74**, 267–274 (1983).
[8] R. Raspet, J. Ezell, and H. E. Bass, "Additional comments on and erratum for 'Effect of finite ground impedance on the propagation of acoustic pulses' [J. Acoust. Soc. Am. **74**, 267–274 (1983)]," J. Acoust. Soc. Am. **77**, 1955–1958 (1985).
[9] J. Nicolas, J.-L. Berry, and G. A. Daigle, "Propagation of sound above a finite layer of snow," J. Acoust. Soc. Am. **77**, 67–73 (1985).
[10] H. Gubler, "Artificial release of avalanches by explosives," J. Glaciology **19**, 419–429 (1977).
[11] M. E. Delaney and E. N. Bazley, "Acoustical properties of fibrous absorbent materials," Appl. Acoust. **3**, 105–116 (1970).
[12] K. Attenborough, S. I. Hayek, and J. M. Lawther, "Propagation of sound above a porous half-space," J. Acoust. Soc. Am. **68**, 1493–1501 (1980).
[13] K. E. Attenborough, "Acoustical characteristics of rigid fibrous absorbents and granular materials," J. Acoust. Soc. Am. **73**, 785–799 (1983).
[14] L. M. Brekhovskikh, *Waves in Layered Media* (Academic, New York, 1980), 2nd ed., p. 17.
[15] K. Attenborough and O. Buser, "On the application of rigid-porous models to impedance data for snow," J. Sound Vib. **124**, 315–327 (1988).
[16] Note that Ref. 15 has a different definition of the pore shape factor ratio using $s_p = 2s_f$. The tabulated values for snow in Attenborough and Buser (Ref. 15) were thus multiplied by 2 for these computations.
[17] ANSI S1.26, "American national standard method for the calculation of the absorption of sound by the atmosphere" (American National Standard Institute, New York, 1978).
[18] D. G. Albert and J. Orcutt, "Observations of low frequency acoustic-to-seismic coupling in the summer and winter," J. Acoust. Soc. Am. **86**, 352–359 (1989).
[19] The snow porosity was estimated from the measured snow density and the pore shape factor from data presented in Attenborough and Buser (Ref. 15). The soil values were taken from an example in Attenborough (Ref. 1).
[20] J. M. Sabatier, H. E. Bass, L. N. Bolen, and K. Attenborough, "Acoustically induced seismic waves," J. Acoust. Soc. Am. **80**, 646–649 (1986).
[21] O. Buser and W. Good, "Acoustic, geometric and mechanical parameters for snow," in *Avalanche Formation, Movement and Effects* (Proceedings of the Davos Symposium, September 1986), edited by B. Salm and H. Gubler (International Association of Hydrological Sciences, Wallingford, UK, 1987), pp. 61–71.